UAV-Borne 3-D Mapping System by Multisensor Integration

Masahiko Nagai, Tianen Chen, Ryosuke Shibasaki, Hideo Kumagai, and Afzal Ahmed

***Abstract*—To represent 3-D space in detail, it is necessary to acquire 3-D shapes and textures simultaneously and efficiently through the use of precise trajectories of sensors. However, there is no reliable, quick, cheap, and handy method for acquiring accurate high-resolution 3-D data on objects in outdoor and moving environments. In this paper, we propose a combination of charge-coupled device cameras, a small and inexpensive laser scanner, an inexpensive inertial measurement unit, and Global Positioning System for a UAV-borne 3-D mapping system. Direct georeferencing is achieved automatically using all of the sensors without any ground control points. A new method of direct georeferencing by the combination of bundle block adjustment and Kalman filtering is proposed. This allows objects to be rendered richly in shape and detailed texture automatically via a UAV from low altitude. This mapping system has been experimentally used in recovery efforts after natural disasters such as landslides, as well as in applications such as river monitoring.**

***Index Terms*—Image orientation analysis, image sensors, inertial navigation, Kalman filtering, lasers, multisensor systems.**

I. Introduction

UTILIZATION of a mobile platform is important for acquiring data effectively over a wide area [1]. Mobile mapping was first developed in the late 1980s. The more recent availability of Global Positioning Systems (GPSs) and inertial measurement units (IMUs), the letter of which is a combination of accelerometers and gyroscopes, has made mobile mapping systems possible, particularly for aerial surveys [2], [3]. Aerial surveying has become a valuable means of mapping and environmental monitoring. Remote sensors—such as image sensors or laser scanners—are instruments that gather information about an object or area from a distance. Although they can cover a wide target area and provide archived data, their spatial and temporal resolution has not always been suitable for detailed mapping.

Ground surveying, on the other hand, is conducted using an instrument called a total station (a small telescope equipped with an electronic distance-measuring device) along with a GPS, a laser scanner, a digital camera, and so on. Since ground surveying is conducted on the ground, it is close to, or on, the observation target. Although this makes it easy to acquire detailed and accurate information, ground surveying tends to be expensive, labor intensive, and time consuming. In disaster areas, it can also be unsafe.

To obtain both the wide-area coverage of remote sensors and the high levels of detail and accuracy of ground surveying, at low cost, we have developed an unmanned aerial vehicle (UAV)-borne mapping system. All the measurement tools are mounted under the UAV, which resembles a helicopter, to acquire detailed information from low altitudes, unlike high-altitude systems in satellites or airplanes. The survey is conducted from the sky, but the resolution and accuracy are equal to those of ground surveying. Moreover, the UAV can acquire data easily as well as safely.

This airborne platform integrates digital and infrared (IR) cameras, a small and cheap laser scanner, an inexpensive IMU, and GPS. These sensors are integrated by a high-precision positioning system designed for moving environments [4]. In this paper, direct georeferencing is achieved automatically from a mobile platform without ground control points. Here, direct georeferencing means georeferencing that does not require ground control points having accurately measured ground coordinate values. Data are acquired, and digital surfaces are modeled using a laser scanner, charge-coupled device (CCD) cameras, GPS, and an IMU, all of which are mounted under the UAV. This allows objects to be rendered in rich shapes and detailed textures automatically.

II. System Design

A. Sensors

In this paper, a laser scanner, CCD cameras (both digital and IR), an IMU, and GPS are used to construct a digital surface model. To automatically construct such a model, it is necessary to develop a high-frequency positioning system to determine the movement of the sensors in details. The integration of GPS and IMU data is effective for high-accuracy positioning of a mobile platform. A 3-D shape is acquired by the laser scanner as point cloud data, texture information is acquired by the digital cameras, and vegetation indexes are acquired by

Manuscript received December 14, 2007; revised June 10, 2008, September 1, 2008, and October 3, 2008. Current version published February 19, 2009. This work is supported in part by the River Fund administered by the Foundation of River and Watershed Environment Management (FORREM), Japan.

M. Nagai is with the Earth Observation Data Integration and Fusion Research Initiative, The University of Tokyo, Japan, 435 Research Centers, CSIS, Chiba 277-8568, Japan (e-mail: nagaim@iis.u-tokyo.ac.jp).

T. Chen is with the Institute of Industrial Science, The University of Tokyo, Tokyo 106-0032, Japan (e-mail: chentian@iis.u-tokyo.ac.jp).

R. Shibasaki and A. Ahmed are with the Center for Spatial Information Science, The University of Tokyo, Chiba 277-8568, Japan (e-mail: shiba@csis.u-tokyo.ac.jp; afzal@iis.u-tokyo.ac.jp).

H. Kumagai is with the Spacetronics Laboratory, Tamagawa Seiki Company, Ltd., Nagano 395-8515, Japan (e-mail: hideo-kumagai@tamagawa-seiki.co.jp).

Color versions of one or more of the figures in this paper are available online at http://ieeexplore.ieee.org.

Digital Object Identifier 10.1109/TGRS.2008.2010314

TABLE I
SENSORS

Sensors	Model	Specifications	Quantity
Digital Camera	Canon EOS 10D	3,072×2,048 pixels Focal length: 24.0mm Price: $1,500US Weight: 500g	2
IR Camera	Tetracam ADC3	2,048×1,536 pixels Green, red, and NIR sensitivity with bands approximately equal to TM2, TM3, and TM4. Focal length: 10.0mm Price: $6,000US Weight: 500g	2
Laser Scanner	SICK LMS-291	Angular resolution: 0.25° Max. distance: 80m Accuracy (20m) : 10mm Price: $4,000US Weight: 4,000g	1
IMU	Tamagawa Seiki Co., Ltd TA7544	Fiber optic gyro Accuracy Angle: ±0.1° Angle velocity: ±0.05°/s Acceleration: ±0.002G Price: $20,000US Weight: 1,000g	1
GPS	Ashtech G12	Accuracy differential: 30cm Velocity accuracy: 0.1(95%) Price: $4,000US Weight: 150g	1

the IR cameras all from the same platform simultaneously. The sensors used in this paper are listed in Table I.

The key attributes of the system design are low cost, ease of use, and mobility [5]. It utilizes a small laser scanner, commercially available digital cameras, and a relatively inexpensive IMU (FOG: fiber-optic gyro). The IMU and other measurement tools used are much cheaper than those in existing aerial measurement systems, such as Applanix's POS and Leica's ADS40 [6]. These low-cost instruments are easy to find on the market. Recent technological advances have also led to low-cost sensors such as microelectromechanical systems (MEMS) gyros. For example, it is considered that MEMS gyros will supplant FOG in the near future and that its price will be one-to-ten that of FOG. That is why we selected FOG ($20 000 U.S.) for this paper to improve a low-cost system in the future. Second, "mobility" here means the item is lightweight and simple to modify. The weight of each sensor is shown in Table I. Such sensors allow the system to be borne by a variety of platforms: UAV, ground vehicles, humans, and so on. These sensors are generally low-performance, but they are light and low cost while still meeting the specifications. These handy sensors are improved by integrating their data.

B. UAV Platform

In this paper, all of the measurement tools are mounted under the UAV, which is a helicopterlike model RPH2 made by Fuji Heavy Industries, Ltd., and shown in Fig. 1. The RPH2 is 4.1 m long, 1.3 m wide, and 1.8 m tall. Table II shows its main specifications. All the sensors are mounted tightly to the bottom of the fuselage.

Fig. 1. RPH2, manufactured by Fuji Heavy Industries, Ltd., with sensors mounted tightly underneath.

TABLE II
SPECIFICATIONS OF RPH2

Weight	330kg
Payload	100kg
Motor	83.5hp
Main rotor	2 rotors, diameter 4.8m
Tail rotor	2 rotors, diameter 0.8m
Operational range	3km or more
Flight time	1 hour
Ceiling	2,000m

As shown in Table II, the RPH2 is quite a large UAV. However, in this paper, it is considered a platform for the experimental development of a multisensor integration algorithm. The RPH2 has a large payload capacity, so it can carry large numbers of sensors, control PCs, and a large battery. After the algorithm is developed, a small UAV system is implemented using selected inexpensive sensors for certain observation targets. This paper focuses on mapping, not UAV system development; this mapping system adapts to any platform.

There are several advantages to utilizing a UAV. One of the most important is that it is unmanned and, therefore, can fly over dangerous zones. This advantage suits the purpose of direct georeferencing in this paper. Direct georeferencing does not require ground control points having accurately measured ground coordinate values. In dangerous zones, it is impossible to set control points, unlike the case in normal aerial surveys. The addition of this direct georeferencing method from a UAV could be an ideal tool for monitoring dangerous situations. Therefore, this UAV-based mapping system is ideally suited for disaster areas such as landslides and floods, and for other applications such as river monitoring.

C. Sensor Setting

All the sensors are tightly mounted under the UAV to ensure that they have a constant geometric relationship during the measurement. The CCD cameras and the laser scanner are calibrated to estimate relative position and attitude [7], [8]. Moreover, all sensors are controlled by a laptop PC and are synchronized by GPS time, one pulse per second. The sensors are set, as shown in Fig. 2. A digital video camera is also

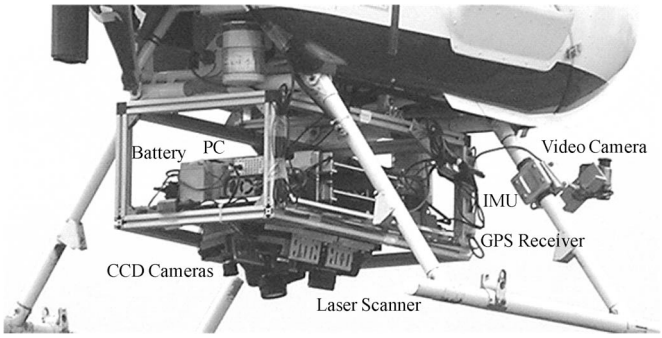

Fig. 2. Arrangement of system components under the UAV.

TABLE III
UAV FLIGHT CONDITIONS

Flight altitude	50m - 150m
Flight speed	1.6m/s
Covered area (in one flight, 15 min)	300m × 500m
Digital camera : covered area	47.3m × 31.5m per camera (at altitude 150m)
Digital camera : ground resolution	1.5cm – 5.0cm (at altitude 50 m - 150m)
Digital camera : overlap	50% (at altitude 150m)
Laser scanner : scan width	120m (at altitude 50m)
Laser scanner : ground resolution	30cm (at altitude 50m)

mounted to sends images to the ground station in real time to monitor the flight course.

D. Experimental Test

The RPH2was rented for the experimental test from Fuji Heavy Industries, Ltd. To ensure safe operation, the RPH2 is controlled by two professional operators and does not fly over people, houses, or cars, in conformance with UAV flight regulations. Moreover, it should be noted that the UAV does not fly if the wind speed is more than 10 m/s.

The UAV flies at a speed of about 1.6 m/s to acquire laser-scanned data with sufficiently fine resolution and sequential CCD camera images with sufficient overlaps for image processing. Table III shows the flight conditions for the experiment. The experiment is conducted at an altitude of 50 m for laser scanning and 150 m for image acquisition. These acquired data are used for the following data processing.

III. MULTI SENSOR INTEGRATION

A. Overview

Fig. 3 shows an overview of data processing. In this paper, the following data are acquired; base station GPS data, remote station GPS data, IMU data, CCD images, and laser range data. Although the data are acquired in different frequencies, they are synchronized with each other by GPS time.

First, differential GPS postprocessing is conducted by Waypoint's GrafNav commercial software, with an accuracy of approximately 30 cm. Second, the processed GPS data and the

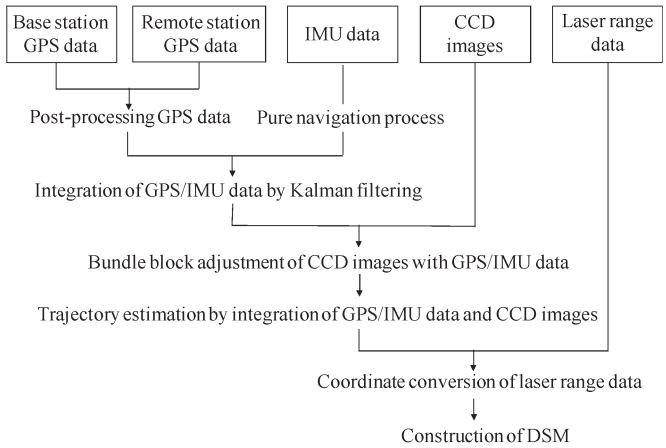

Fig. 3. Overview of data processing for multisensor integration. Those procedures are conducted by postprocessing.

Fig. 4. Multiple cameras set to capture a wide area from low altitude.

IMU data are integrated by Kalman filtering to estimate the sensor trajectory. The bundle block adjustment (BBA) of the CCD images is then made to acquire georeferenced images and exterior orientations with the support of GPS and IMU data, which are the sensor position and attitude. Finally, GPS data, IMU data, and the result of the BBA are combined to regenerate high-precision and time-series sensor position and attitude. Then, these hybrid positioning data are used for the coordinate conversion of the laser range data and for the construction of a digital surface model as 3-D point cloud data.

B. Multiple Cameras

To cover a wide area from low altitude, multiple cameras are mounted under the UAV. In this paper, two digital cameras and two IR cameras are mounted in parallel at certain fixed angles. These CCD sensors are tightly mounted on a hard aluminum plate to have a constant geometric arrangement during the experiment, as shown in Fig. 4. Calibrations of CCD cameras are calculated by taking calibration targets before the experiment for estimating interior orientation parameters such as focal length, lens distortion, principle points, and the external orientations of four CCD cameras. As the result of camera calibration, average error of image coordinate is 0.06 pixel, and this result is adequate for the BBA.

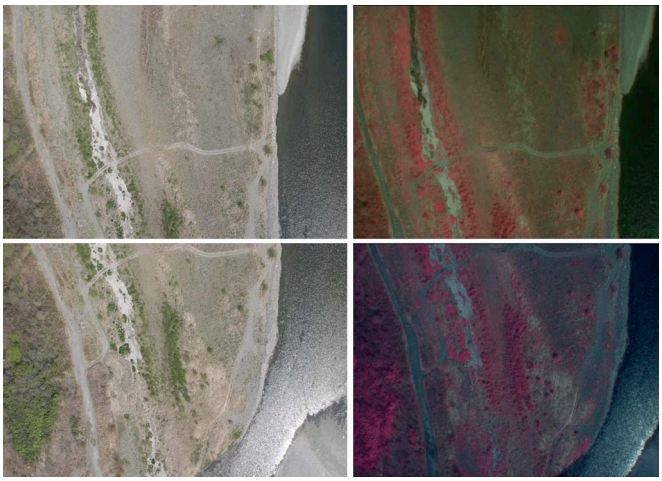

Fig. 5. Images acquired by four CCD cameras simultaneously.

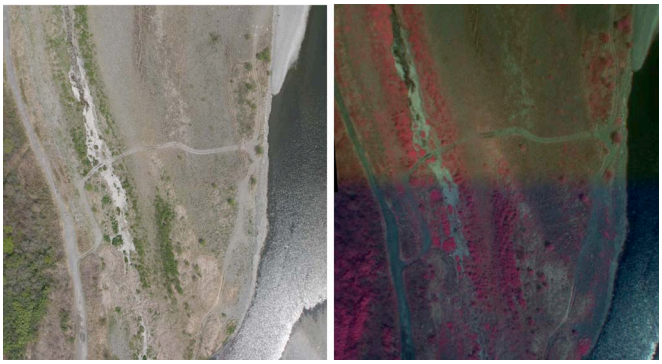

Fig. 6. Mosaicked images acquired by four CCD cameras.

Four images are acquired at the same time, as shown in Fig. 5. Those images are rectified by using calibration data. The rectified images are mosaicked by the GPS data. Image overlap for mosaicking is estimated by altitude information from the GPS data. Then, image matching of the overlapped area is conducted and a mosaic image is constructed. Mosaic images can thus capture a wide area even at low altitude, as shown in Fig. 6. These mosaicked images are used for further image processing steps.

C. GPS/IMU Integration by Kalman Filtering

The GPS and IMU data are integrated by Kalman filtering. The Kalman filter can be used to optimally estimate the system states. With this filter, the final estimation is based on a combination of prediction and actual measurement. Fig. 7 shows the pure navigation algorithm for deciding attitude, velocity, and position step by step [9]. Inertial navigation starts to define the initial attitude and heading based on the alignment of the system. Its process then changes to the navigation mode. The quality of IMUs has risen, but they are still affected by systemic errors. Here, GPS measurement is applied as actual measurement to aid the IMU by correcting this huge drift error. Through Kalman filtering, the sensor position and attitude are determined at 200 Hz.

Fig. 8 shows the Kalman filter circulation diagram for the integration of the GPS and IMU data [10]. Individual measurement equations and transition equations are selected, and covariance must be initialized in order to continue Kalman filtering circulation in response to the GPS data validation. The accuracy of the integration depends on the accuracy of the referenced GPS. In this case, it is approximately 30 cm.

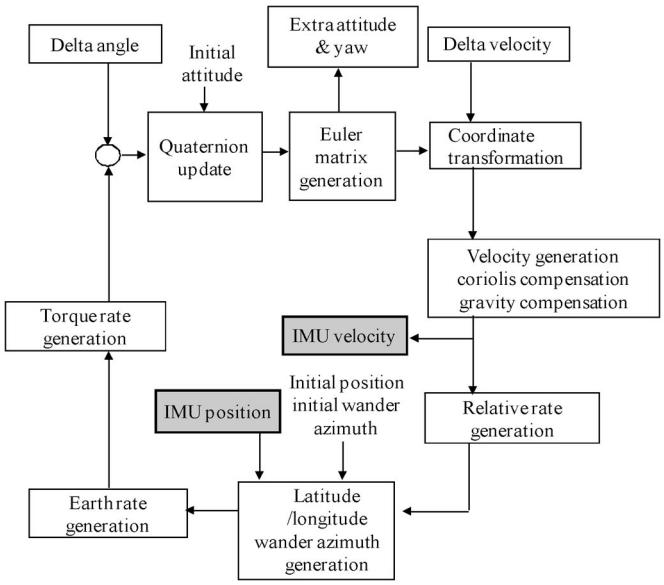

Fig. 7. Pure navigation block diagram expressed roughly step by step.

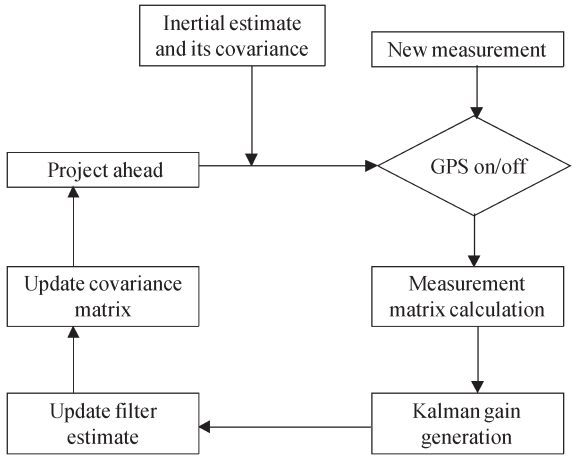

Fig. 8. Kalman filter circulation.

In addition, a boresight offset must be estimated between the GPS and the IMU. In the Kalman filter circulation, differences in position and velocity between the IMU and the GPS are used to estimate the severity of errors. If the UAV just goes straight, this error amount is not affected because the relative movement is constant. However, if the UAV turns, the error amount is not constant. The position and velocity of the near axis of gyration are small, although those of its far axis of gyration are large. In this paper, the boresight offset from the GPS to the IMU in the UAV is obtained through direct measurement by using the total station.

D. BBA of CCD Images

Meanwhile, the image exterior orientation is determined by BBA for the mosaicked CCD images. The BBA is a nonlinear

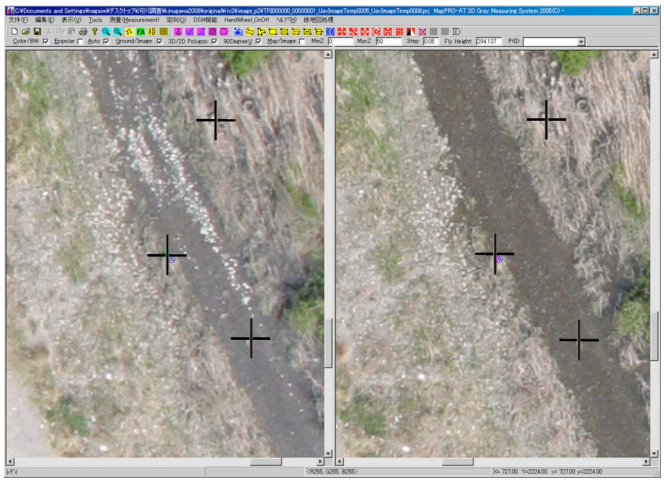

Fig. 9. Image orientation with tie points.

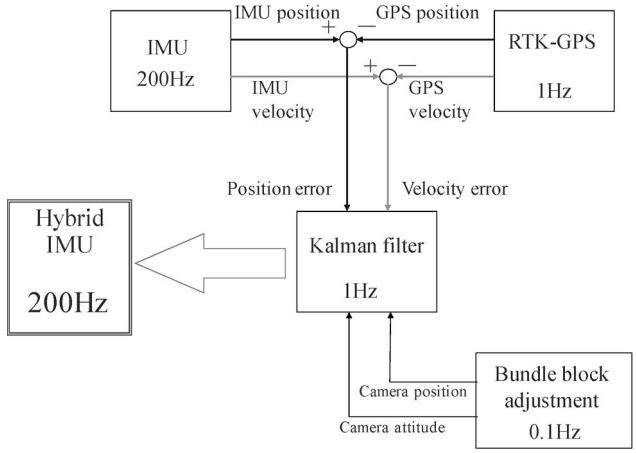

Fig. 10. Strapdown navigation algorithm for hybrid IMU.

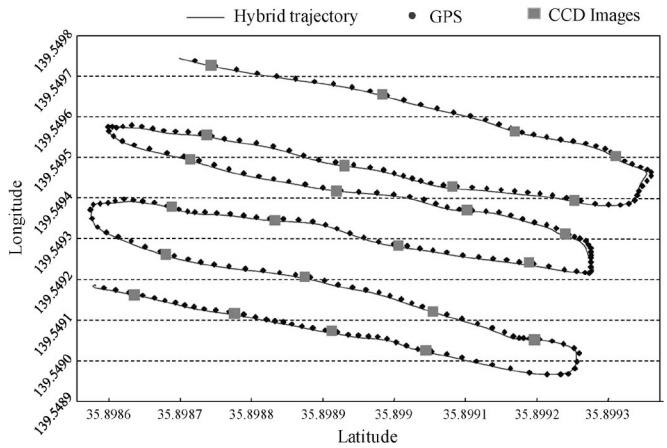

Fig. 11. Trajectory of UAV by hybrid IMU with GPS and image orientations.

least squares optimization method using the tie points of the inside block [11]. Bundle block configuration increases both the reliability and accuracy of object reconstruction. An object point is determined by the intersection of more than two images, which provides local redundancy for gross error detection and which consequently forms a better intersection geometry [12]. Therefore, in this paper, the CCD images are set to overlap by more than 50% in the forward direction, and by more than 30% on each side. The GPS and IMU data obtained in a previous step allow the automatic setting of tie points in overlapped images and reduce the time spent searching for tie points by limiting the search area based on the epipolar line. The epipolar line is the straight line of intersection between the epipolar plane and the image plane, and it is estimated by the sensor position and attitude, which is derived from GPS/IMU integration. It connects the image point in one image through the image point in the next image. Fig. 9 shows an image orientation series with tie points that overlap each other. The image resolution is extremely high (approximately 1.5 cm), so it is easy to detect small gaps or cracks.

The accuracy of the image orientation is estimated by comparison with 20 control points. The average error of the plane is approximately 3 to 6 cm. The average error of the height is approximately 10 cm. That is, although the BBA is done automatically, the result is very accurate compared with the differential GPS or the GPS/IMU integration data, in which the average error is approximately 30 cm. Moreover, processing time is very short; for example, it takes 20 min to process 40 images by the BBA. Thus, the BBA results aid Kalman filtering by initializing the position and attitude in the next step to acquire a much more accurate trajectory.

E. Positioning by Multisensor Integration

The position and attitude of the sensors are decided by the integration of the GPS and IMU data, as well as by the CCD image orientation. One of the main objectives of this paper is to integrate inexpensive sensors into a high-precision positioning system. Integration of the GPS (which operates at 1 Hz) with the IMU (200 Hz) has to be made with Kalman filtering for the georeferencing of laser range data with a frequency of 18 Hz. The positioning accuracy of the GPS/IMU integration data is approximately 30 cm. On the other hand, position and attitude can be estimated with very high accuracy using the BBA of the CCD images, although the images are taken every 10 s.

Therefore, the combination of BBA and Kalman filtering is conducted to increase accuracy. The BBA results are assumed to be true position values. They provide initial attitude and heading without any alignment. The IMU are initialized by Kalman filtering using the BBA result every 10 s. That is, after every computation of the BBA, the IMU data and their error are corrected. Fig. 10 shows the strapdown navigation algorithm for the GPS/IMU integration and the BBA result. The combination of GPS, IMU, and CCD images can be called "hybrid IMU."

As a result of the multisensor integration, the trajectory of the hybrid IMU can assure sufficient georeferencing accuracy for the CCD images. The trajectory of the CCD sensors can be representative of the trajectory of the platform because the GPS and IMU data are initialized by camera orientation. This is one of our system's advantages. Their coordinate is fitted to the CCD sensors' coordinate. Fig. 11 shows the trajectory of the UAV in this experiment. The light-gray squares are the orientation of CCD images by the BBA, and these points initialize the Kalman filtering. The dark-gray circles form the trajectory of the differential GPS. The line is the hybrid IMU.

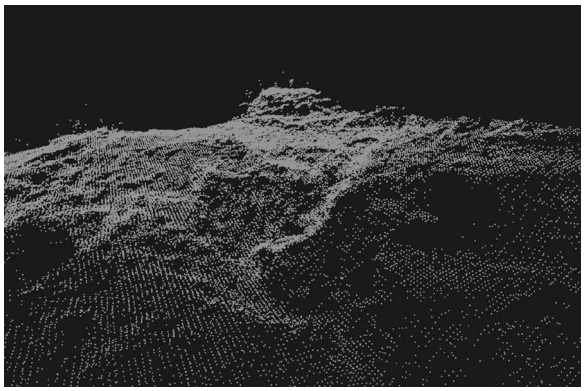

Fig. 12. Three-dimensional point cloud data by direct georeferencing of laser range data.

IV. Digital 3-D Model

A. Direct Georeferencing

During measurement, the platform including all of the sensors is continuously changing its position and attitude with respect to time. For direct georeferencing of laser range data, the hybrid IMU data are used. There are two coordinate systems: that of the laser scanner and that of the hybrid IMU, WGS84 (world geodetic system 1984) based on GPS data. It is necessary to transform the laser scanner coordinate into the WGS84 coordinate by georeferencing. Georeferencing of the laser range data is determined by the 3-D Helmert's transformation, which is computed by the rotation matrix and shift vector with the hybrid IMU data and calibration parameters as offset values. The offset values from the laser scanner to the digital cameras in the body frame are already obtained by the sensor calibration.

All the points scanned by the laser scanner (x) are transformed into the WGS84 (X_{w}), which is the same as the digital camera coordinates system as given in (1). To correct drift error, the rotation matrix (R_{h}) and shift vector (S_{h}) from the hybrid IMU are used with respect to time. Offset values ($R_{\mathrm{l}-d}$ and $S_{\mathrm{l}-d}$) are already estimated in sensor calibration.

$$X_{\mathrm{w}} = (R_{\mathrm{h}} * R_{\mathrm{l}-d})\, x + (S_{\mathrm{h}} + S_{\mathrm{l}-d}) \tag{1}$$

where

R_{h}, S_{h} hybrid IMU, rotation and shift;
$R_{\mathrm{l}-d}$, $S_{\mathrm{l}-d}$ offset by calibration.

Georeferencing of laser range data and CCD images is done directly. Fig. 12 shows the 3-D point cloud data that are directly georeferenced by the hybrid IMU data. In this paper, the WGS84 is used as the base coordinate system for the 3-D point cloud data.

B. Color Rendering

The digital surface model, a 3-D model of the object surface, is manipulated. It is comprised of 3-D measurements that are laid out on colored point clouds. These measurements use the 3-D point cloud data derived from the laser range data, along with the texture data derived from the CCD images.

The point cloud data acquired by the laser scanner is georeferenced by the hybrid IMU data. The hybrid IMU data

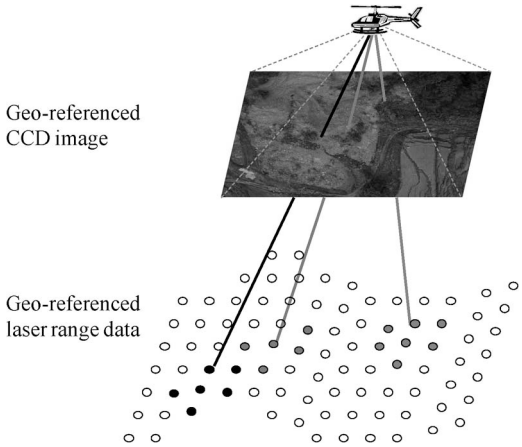

Fig. 13. Concept of color rendering of 3-D point cloud data.

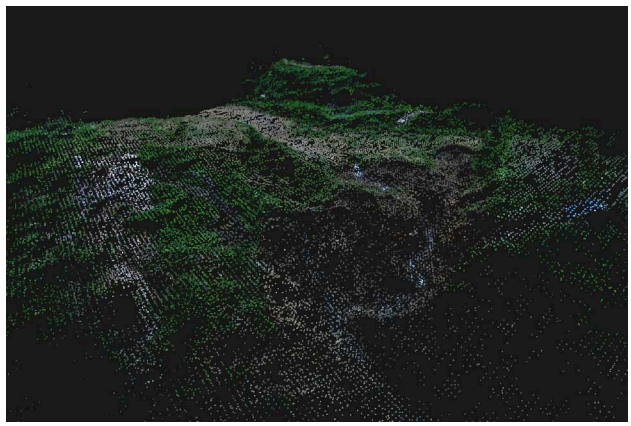

Fig. 14. Digital surface model with texture from CCD images.

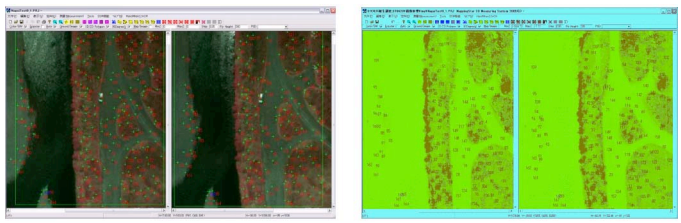

Fig. 15. Processing of IR camera images and NDVI images.

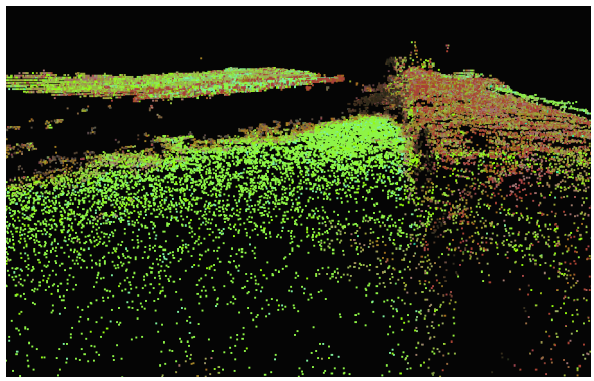

Fig. 16. Three-dimensional vegetation index model.

TABLE IV
ACCURACY OF DIGITAL SURFACE MODEL

Unit: m

No.	Control point from Image (X)	(Y)	(Z)	DSM (X)	(Y)	(Z)	Error (X)	(Y)	(Z)
1	-11184.877	-25630.253	42.755	-11184.696	-25630.836	42.915	0.181	0.583	0.160
2	-11185.471	-25622.727	42.952	-11185.557	-25622.789	42.971	0.086	0.062	0.019
3	-11167.603	-25670.474	42.391	-11168.282	-25670.312	42.406	0.679	0.162	0.015
4	-11177.107	-25634.721	42.704	-11177.262	-25634.918	42.523	0.155	0.197	0.181
5	-11152.866	-25641.753	42.029	-11152.172	-25641.036	42.071	0.694	0.717	0.042
6	-11176.511	-25625.571	42.824	-11176.467	-25625.426	42.767	0.044	0.145	0.057
7	-11153.911	-25643.823	42.534	-11154.375	-25643.041	42.075	0.464	0.782	0.459
8	-11150.564	-25631.724	42.340	-11150.887	-25631.869	42.296	0.323	0.145	0.044
9	-11176.771	-25635.344	43.992	-11176.394	-25635.308	44.082	0.377	0.036	0.090
10	-11186.666	-25631.657	44.289	-11186.417	-25631.888	44.202	0.249	0.231	0.087
						Ave. Error	0.325	0.306	0.115

are computed based on the BBA of CCD images. Texture data are overlaid on the georeferenced point cloud data. The integrated point cloud data match the image data well, since the hybrid IMU data are initialized by the result of the BBA of the sequential image data. Moreover, the relative orientation of the CCD cameras and the laser scanner is done before the experiment.

Fig. 13 shows the concept of color rendering of 3-D point cloud data. Each point in the georeferenced laser point data corresponds to a pixel in the georeferenced CCD image in the same coordinate system. In this paper, 3-D point cloud data take on well the color of the corresponding image pixels for a textured digital surface model, as shown in Fig. 14. In the case of landslides, 3-D point cloud data with detailed images can help us understand the damage and estimate the volume of soil moved by deriving a triangulated irregular network.

C. Vegetation Index

As shown in Fig. 15, IR camera images are processed in the same manner as the digital cameras. After image orientation calculated in the IR images, normalized difference vegetation index (NDVI) is calculated to determine the density of plants by observing the distinct colors (wavelengths) of visible and near-IR sunlight reflected.

The laser range data and the IR camera images correspond to each other. The vegetation index is then applied to the digital surface model. The 3-D point cloud data take on colors from the corresponding NDVI images. Fig. 16 shows the 3-D vegetation index model. In the case of river monitoring, 3-D point cloud data with NDVI help in the estimation of vegetation volume.

D. Accuracy Assessment

In this mapping system, multiple sensors are integrated, so it is difficult to point out the origins of errors. Therefore, accuracy is assessed by an ordinary survey method, the result of which is compared with digital surface model and control points from the oriented images; the accuracy is 3 to 10 cm, as shown in Table IV. Control points are ten selected feature points such as object corners, which can recognize both images and digital surface model (DSM). As a result, the average error of the digital surface model is approximately 10 to 30 cm, as shown in Table IV. Moreover, the georeferenced laser range data and CCD images are recognized to match each other by using the control points.

The laser range data are acquired from 50 m altitude and the scan angler resolution is 0.25°; that is, the density of 3-D laser points is about 20 to 30 cm^2. Comparing mapping accuracy with the laser point density, the accuracy is good enough by considering automatic data processing from the UAV.

V. CONCLUSION

A digital surface model was constructed by integrating entirely inexpensive sensors—a laser scanner, CCD cameras, IMU, and GPS. A new method of direct georeferencing was proposed for laser range data and CCD images by combining Kalman filter and the BBA. Because the BBA avoids the accumulation of drift error in the Kalman filtering, the georeferenced laser range data and the CCD images were overlapped properly in the common world coordinate system automatically. All the sensors and instruments were assembled and mounted under a UAV in this experiment. This paper focused on how to integrate these sensors into a UAV platform. Finally, the precise trajectory of the sensors was computed as the hybrid IMU for direct georeferencing. The hybrid IMU is used to construct digital surface models with texture as well as with a vegetation index for monitoring landslides and rivers.

In the future, a small UAV system with selected sensors will be implemented for certain observation targets. It is expected that this system will help us understand geographic features in detail easily and safety.

REFERENCES

[1] H. Zhao and R. Shibasaki, "Reconstruction of textured urban 3D model by fusing ground-based laser range and CCD images," *IEICE Trans. Inf. Syst.*, vol. E83D, no. 7, pp. 1429–1440, 2000.
[2] *Handbook of Airborne Laser Scanners*, Assoc. Precise Survey Appl. Technol., Tokyo, Japan, 2004.
[3] D. Manandhar and R. Shibasaki, "Auto-extraction of urban features from vehicle-borne laser data," in *Proc. ISPRS GeoSpatial Theory, Process. Appl.*, Ottawa, ON, Canada, 2002.
[4] M. Nagai and R. Shibasaki, "Robust trajectory tracking by combining GPS/IMU and continual CCD images," in *Proc. 25th Int. Symp. Space Technol. Sci.*, Kanazawa, Japan, 2006, pp. 1189–1194.
[5] S. Parra and J. Angel, "Low cost navigation system for UAV's," *Aerosp. Sci. Technol.*, vol. 9, no. 6, pp. 504–516, Sep. 2005.

[6] M. Cramera, "The ADS40 Vaihingen/Enz geometric performance test," *ISPRS J. Photogramm. Remote Sens.*, vol. 60, no. 6, pp. 363–374, Sep. 2006.
[7] Y. Kunii and H. Chikatsu, "Application of 3-million pixel armature camera for the 3D modeling of historical structures," *Asian J. Geoinformatics*, vol. 2, no. 1, pp. 39–48, 2001.
[8] R. Shapiro, "Direct linear transformation method for three-dimensional cinematography," *Res. Q.*, vol. 49, no. 2, pp. 197–205, May 1978.
[9] H. Kumagai, Y. Kubo, M. Kihara, and S. Sugimoto, "DGPS/INS/VMS integration for high accuracy land-vehicle positioning," *J. Jpn. Soc. Photogramm. Remote Sens.*, vol. 41, no. 4, pp. 77–84, 2002.
[10] H. Kuamgai, T. Kindo, Y. Kubo, and S. Sugimoto, "DGPS/INS/VMS integration for high accuracy land-vehicle positioning," in *Proc. Inst. Navig. ION GPS*, Salt Lake, UT, 2000, pp. 1845–1853.
[11] M. Takagi and H. Shimoda, *Handbook of Image Analysis*. Tokyo, Japan: Univ. Tokyo Press, 2004.
[12] T. Chen, R. Shibasaki, and S. Murai, "Development and calibration of the airborne three-line scanner (TLS) imaging system," *Photogramm. Eng. Remote Sens.*, vol. 69, no. 1, pp. 71–78, 2003.

Masahiko Nagai received the B.S. degree in chemistry from St. Cloud State University, St. Cloud, MN, the M.S. degree in remote sensing and geographic information science from the Asian Institute of Technology, Bangkok, Thailand, in 2002, and the Doctoral Degree of Eng. in civil engineering from The University of Tokyo, Tokyo, Japan, in 2005.

He is an Assistant Professor with The University of Tokyo. His current research focuses on the development of ontological information as an interoperability arrangement, as well as the construction of 3-D modeling by integrating multiple sensors.

Tianen Chen received the B.S. and M.S. degrees in photogrammetry and remote sensing from Wuhan Technical University of Surveying and Mapping, Wuhan, China, in 1988 and 1995, respectively, and the Ph.D. degree in civil engineering from The University of Tokyo, Tokyo, Japan, in 1999.

He is an Assistant Professor with The University of Tokyo. His current activities are focused on the calibration of digital optical systems, improvement of airborne linear imagery positioning accuracy, and semi- or fully automatic construction of 3-D cities with multisensor data.

Ryosuke Shibasaki received the B.S., M.S., and Doctoral of Eng. degrees in civil engineering from The University of Tokyo, Tokyo, Japan, in 1980, 1982, and 1987, respectively.

He is a Professor and a Director with the Center for Spatial Information Science, The University of Tokyo. From 1982 to 1988, he was with the Public Works Research Institute, Ministry of Construction. From 1988 to 1991, he was an Associate Professor of civil engineering with The University of Tokyo.

Hideo Kumagai received the Ph.D. degree in electrical and electronic engineering from Ritsumeikan University, Kyoto, Japan, in 2003.

He is a Director for the development of inertial sensors and integrated navigation systems with Spacetronics Laboratory, Tamagawa Seiki Company, Ltd., Nagano, Japan.

Afzal Ahmed received the B.Sc. degree in civil engineering from Bangladesh University of Engineering and Technology, Dhaka, Bangladesh, in 1998 and the M.E. degree in civil engineering from The University of Tokyo, Tokyo, Japan, in 2001, where he is currently working toward the Ph.D. degree.

His current research focuses on developing unmanned aerial vehicle-borne systems for conducting search-and-rescue operation in disaster areas.